# Charge detection mass spectrometry on human-amplified fibrils from different synucleinopathies.

Aikaterini Tsirkou,[a] Flora Kaczorowski,[b,c] Mathieu Verdurand,[b,c] Rana Raffoul,[a] Jonathan Pansieri,[d] Isabelle Quadrio,[b,c] Fabien Chauveau[*,c] and Rodolphe Antoine[*,a]

[a].Univ Lyon, Université Claude Bernard Lyon 1, CNRS, Institut Lumière Matière, F-69622 Lyon, France

E-mail: rodolphe.antoine@univ-lyon1.fr

[b].Laboratory of Neurobiology and Neurogenetics, Department of Biochemistry and Molecular Biology, Lyon University Hospital, 69677 BRON Cedex, France and Center for Memory Resources and Research, Lyon University Hospital, Lyon 1 University, Villeurbanne, France

[c].Univ Lyon, Centre de Recherche en Neurosciences de Lyon, Equipe BIORAN, Inserm U1028 - CNRS UMR5292, Université Claude Bernard Lyon 1, Groupement Hospitalier Est – CERMEP, 69677 BRON Cedex, France E-mail: chauveau@cermep.fr

[d].Oxford University, Nuffield Department of Clinical Neurosciences, Oxford University | Visiting Address : Level 1 Neuropathology, John Radcliffe Hospital, West Wing Oxford OX3, U.K.

# SUPPORTING INFORMATION

## METHODS

**Selection of synucleinopathies patients' brain homogenates.** Human brain tissues were obtained as frozen samples from the London Neurodegenerative Diseases Brain Bank.[1] Medulla oblongata was chosen because this brainstem region is systematically affected during the course of synucleinopathies. All cases used had been examined histologically and the diagnosis reached using internationally accepted criteria.[2] Demographic information provided by the brain bank included age, gender, post-mortem delay, clinical diagnosis, pathology, Thal stage, CERAD stage, Braak tangle stage, presence of αSyn in the medulla oblongata, Braak LB stage, neuropathological diagnostic details, and are presented in Table S1 below.

**Brain homogenate preparations.** Brain homogenates (BH; 10% w/v) were prepared by homogenizing the tissue in phosphate-buffered saline (PBS 1X, VWR Chemicals) containing silica beads, 1 mM EDTA, 150 mM NaCl, 0.5% Triton X-100, and complete protease inhibitor cocktail EDTA-free (Roche) using a ribolyser (BioRad ribolyser TeSeE precess 24). The homogenate was then spun at 2000 g for 2 min at room temperature and the supernatant was transferred to a new tube and stored at -80°C for RT-QuIC (real-time quaking-induced conversion) analysis. For αSyn RT-QuIC testing, BHs were serially diluted in PBS (phosphate buffered saline 1X, VWR Chemicals).

**Protocol for real-time quaking-induced conversion (RT-QuIC).** RT-QuIC reactions were performed in black 96-well plates with a clear bottom (Thermo Fischer Scientific). Plates were preloaded with 10 ± 2 zirconia/silica beads (0.5 mm in diam, BioSpec Products) per well. For each BH tissue, a volume of 2 µL of a $10^{-4}$ dilution was added to wells containing 98µL of the reaction mix to give final concentrations of 40mM phosphate buffer (pH 8.0), 170 mM NaCl, 0.1 mg/mL of commercial human full-length recombinant αSyn (from rPeptide and Roboscreen, filtered through a 100 kDa MWCO filter; Microcon, Merck Millipore), and 10 µM ThT. All patients were run in quadruplicates and tested with both the Roboscreen and rPeptide recombinant proteins. The plate was then sealed with a plate sealer film (Nalgene Nunc International) and incubated at 42°C in a BMG FLUOstar Omega plate reader with cycles of 1 min shaking (400 rpm double orbital) and 1 min rest throughout the indicated incubation time. ThT fluorescence measurements (450 excitation and 480 emission) were taken every 45 min. To overcome the instrinsic experimental variability of RT-QuIC experiments, relative fluorescence unit

(RFU) for every time point were normalized for the maximum of the intensity of the plate and expressed as a percentage (% fluo max). Samples were run in quadruplicate and considered positive when at least two out of four replicates reached the threshold or cutoff, separately calculated for each plate and for each recombinant protein, as the average normalized fluorescence value of the first 10 hours of the run of the CTL BHs samples, plus 10 standard deviations.

**Nanospray-charge detection mass spectrometry.** MS experiments were performed on the custom-built charge-sensing mass spectrometer coupled with a nanospray source. To each well containing 2µL of RT-QuIC fibril stock solution (8.92 µM total αSyn concentration), 10µL of water/acetonitrile (50/50 v/v) was added to achieve an approximate concentration value of 1.49-2.06 µM.
The charge detection mass spectrometry (CDMS) instrument was described in details earlier.[3-4] The mass spectrometer operating in the positive mode was equipped with a customized Nanospray (nESI) Flex Ion Source (Thermo Fisher Scientific) as shown in Figure S1. Electrosprayed ions are guided up the terminal vacuum stage chamber which contains the charge detection device (CDD) to work in a single-pass mode.[5-6] The efficiency of nano-electrospray ionization was reported to be at maximum 12%.[7] The CDD consists of a conductive tube collinear to the ion beam and connected to a field-effect transistor (JFET). The picked up signal is amplified by a low-noise charge-sensitive preamplifier and then shaped and differentiated by a home-built amplifier. The signal is recorded, with a waveform digitizer card. The data are transferred to a desk-top computer where they are analyzed with a custom-written user program. Calibration in charge was performed using a test capacitor that allowed a known amount of charge to be pulsed onto the pick-up tube. An ionic train device composed of multipole radiofrequency (RF) ion guides, permits the transfer of ions (in the optimal $10^2$–$10^5$ m/z window of transmission) through the capillary interface of the nanoelectrospray ionization source to the charge detection device. The nanospray ionization has been customized to fit the entrance of the CDMS instrument. Ion source consists of a housing with manual XYZ-manipulator and fittings, a Direc Junction adaptor for online analysis and a camera set-up including one LCD monitor. Electrospray Fused Silica PicoTips (with ~30 µm tip inner diameter) were used and changed for each sample analysis.

**Optimization of the nanospray-charge detection mass spectrometry set-up with α-lactalbumin fibrils**. Since a low quantity of fibrillar structures present in the tissues of patients with neurodegenerative diseases was extracted from real-time quaking-induced conversion, the optimization of mass spectrometry settings was performed using well-documented α-lactalbumin (α-lac) fibrils, which were already characterized by electrospray ionization source.[8] α-lac fibrils were produced as described earlier.[8] The kinetics of fibril formation were followed by fluorescence of thioflavin T. The measurements performed on the different protein solutions all show an increase in fluorescence intensity. The plateau indicates that mature fibrils are present at the end of the reaction. For 100 mM NaCl, the fibrils are formed in about 30 hours.
Since flow rates are quite different between electrospray (typically 5-10 µL/min) and nanospray (lower than 100 nl/min), the spray mechanism involved in the ionization and gas phase production of fibrils might be different with new adjustable parameters (applied electric field voltage, counterflow of heated nitrogen drying gas, …). Our experimental conditions allow for the addition of a counter flow of heated nitrogen drying gas (typically up to 200°C) within the entrance electrode. Hence, the nitrogen pressure and temperature in the source and the distance between the tip and the end-cap should be chosen carefully in order to enhance desolvation for producing enhanced ions from fibrils samples. It was found that contrary to previous electrospray studies, adding a counterflow of heated nitrogen drying gas (typically up to 200°C) within the entrance electrode induce to unstable ion signal and fragmentation of fibrils for α-lac fibrils used as standard fibrils. A stable signal (for several tens of minutes) for all fibrils under investigation was found without adding any counterflow of heated

nitrogen drying gas and a spray voltage of ~1.2-1.5 kV. The 2D graph (charge vs. mass) shown in Figure S1 reports mass measurements on α-lac fibrils. Both the overall mass and charge distributions are in good agreement with the previously reported data by electrospray CDMS.[8]

In general, one may be concerned that the conditions of ESI are too harsh with diluting in water/acetonitrile solvent mixture before injection into the ESI source. CDMS experiments on α-lac fibrils were performed in two conditions with and without organic solvent, acetonitrile. Mass and charge distribution of samples are little affected by the solvent mixture which indicates that small amounts (inferior to 50 %) of organic solvent do not disrupt the fibrils overall population. In our case, the studied fibrils are very stable and the addition of acetonitrile should not affect their conformation during the time of the MS measurements. Note however, that the ion signal in pure water is very unstable (due to unstable spray) and the addition of acetonitrile allows for both a better ion counting rate, lower spray voltage and a better stability of the spray (see Fig. S1b with a solvent-dependent study performed on α-lac fibrils).

**Transmission electron microscopy.** Transmission electronic microscopy (TEM) was used to detect the presence of fibrils. Sample of fibrils from RT-QuIC (3 µL) was absorbed on 200 mesh nickel grids coated with formvar-C for 2 minutes at room temperature (RT). A torn edged of hardened, ashless filter paper was applied at the edge of the grid to absorb the remaining liquid. Then, grids with suspension were colored with 2% phosphotunstic acid for 2 min and observed on a transmission electron microscope (Jeol 1400 JEM, Tokyo, Japan) operating at 100kV equipped with a numeric camera (GATAN Orius 1000, Evry, France). The images were processed by Digital Micrograph.

Lengths of amyloid fibrils were manually measured on two-to-five TEM pictures for each sample by using ImageJ software. Clusters of fibrils were not considered. Histograms of TEM fibril lengths were built up by using GraphPad Prism software, where bin size was fixed at 25 nm. Each data set was represented by its relative frequency, i.e. each number of fibrils falling in a bin is divided by the total number of fibrils in the sample. This procedure was applied to all experimental data sets.

| **Etiology** | **CTL** | **PD-1** | **PD-2** | **PD-3** | **DLB-1** | **DLB-2** |
|---|---|---|---|---|---|---|
| **Sample name** | NA | A8, B8, C8, D8 | C5/F5 | C6/G6 | B9, C9, D9, F9 | B9/H9 |
| **Age (y)** | 73 | 74 | 72 | 89 | 80 | 81 |
| **Gender** | Female | Male | Male | Female | Female | Male |
| **PM Delay (hrs)** | 27 | 10 | 29 | 18 | 8.5 | 18 |
| **αSyn in the Medulla** | No | Yes | Yes | Yes | Yes | Yes |
| **NPath Diag Details** | Early ageing changes, BNE stage 1, Control | Parkinson's Disease; Minor cerebrovascular disease | Parkinson's Disease | Parkinson's Disease, Cerebrovascular disorder | Severe neocortical LB disease; AD intermediate Braak IV | Neocortical Lewy Body disease, Braak LB stage 6 |

**Table S1**. Patients' characteristics for Figure 2 and S3. AD: Alzheimer's disease; CTL: Control patient; PD: Parkinson's disease; DLB: Dementia with Lewy-body disease; PM delay: post-mortem delay; NPath Diag Details: neuropathological diagnosis details; BNE stage: BrainNet Europe staging system.[9] *NA*: not applicable.

| Sample | Mean mass (MDa) | PDI | Mean charge (ze) |
|---|---|---|---|
| PD | 170 | 1.26 | 530 |
| DLB | 218 | 1.23 | 635 |

**Table S2**: Summary of CDMS analysis presented in the main text. Mean charge and mass as well as PDI are extracted from the lognormal analysis of mass distribution (see Fig. 2).

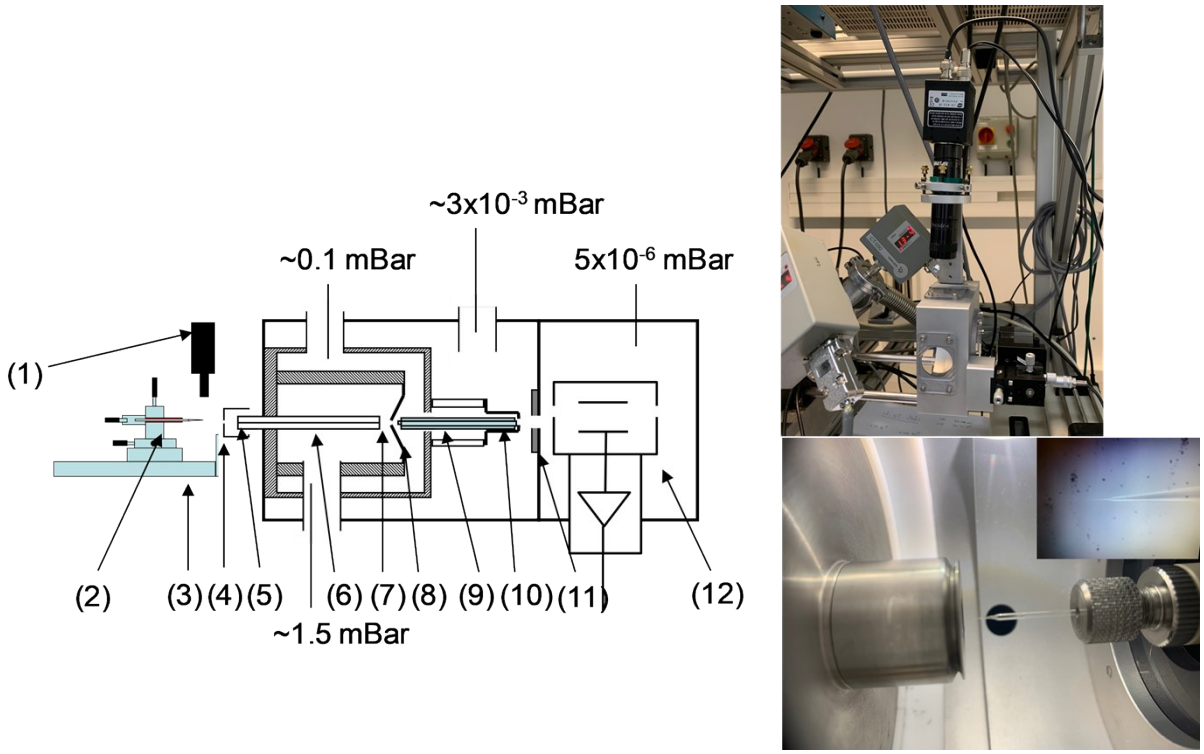


**Figure S1a.** (left) Schematic diagram of the CDMS instrument. The nano-ESI source and vacuum interface generate the ion beam directly toward the charge detector. (1) camera, (2) nanospray tip, (3) XYZ translation stages, (4) end cap, (5) Pt-coated capillary, (6) Pyrex capillary, (7) L1 lens, (8) L2 skimmer, (9) hexapole, (10) L6 exit lens, (11) inter lens, (12) CDD charge detection device. (right) potographs of the customized nanospray, with details on the nanospray tip.

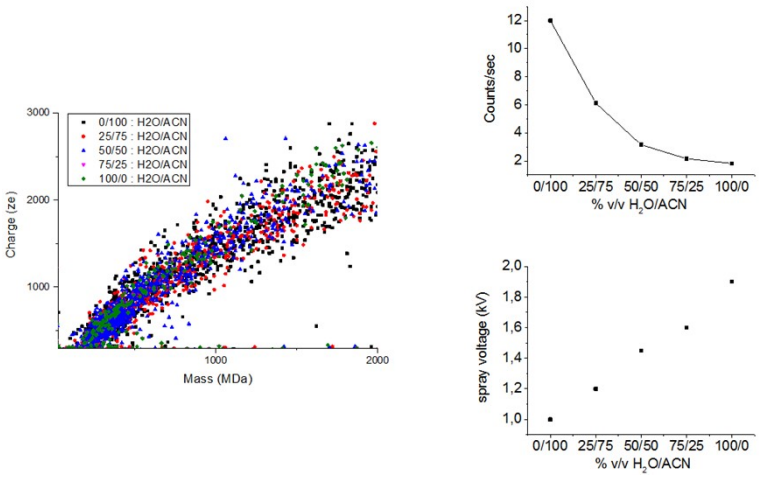


**Figure S1b.** Solvent-dependent CDMS analysis for α-lac fibrils.

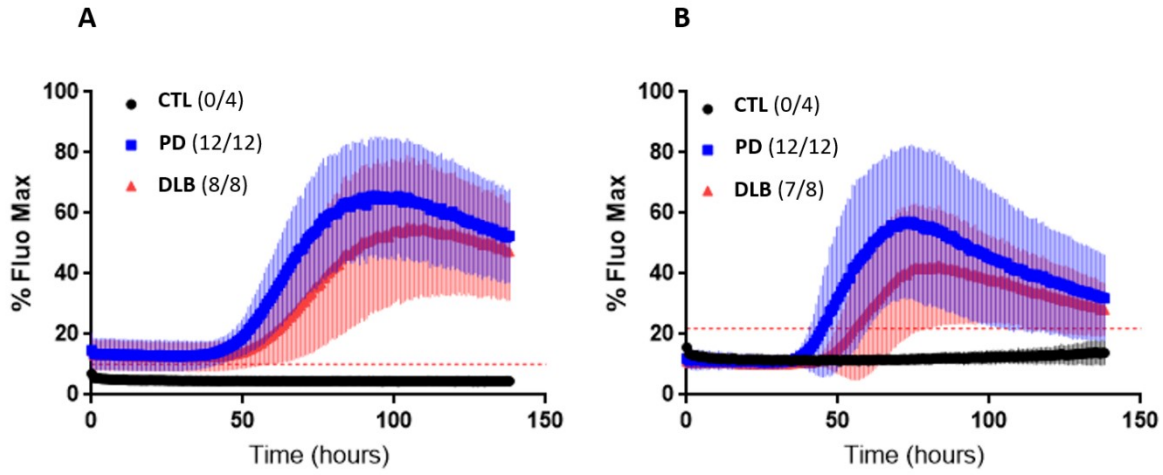


**Figure S2.** Normalized fluorescence average curves during RT-QuIC experiments. The same patients' brain homogenates were run in quadruplicates with each recombinant αSyn protein (**A**, Roboscreen; **B**, rPeptide). Means are represented with standard deviations, and cutoffs showed as a dotted bar. CTL: control patients (n = 1); PD: Parkinson's Disease patients (n = 3); DLB: dementia with Lewy Bodies (n = 2). Number of replicates above the threshold/cutoff at 100 hours of lag-phase is mentioned between brackets on the graph's legend for each etiology.

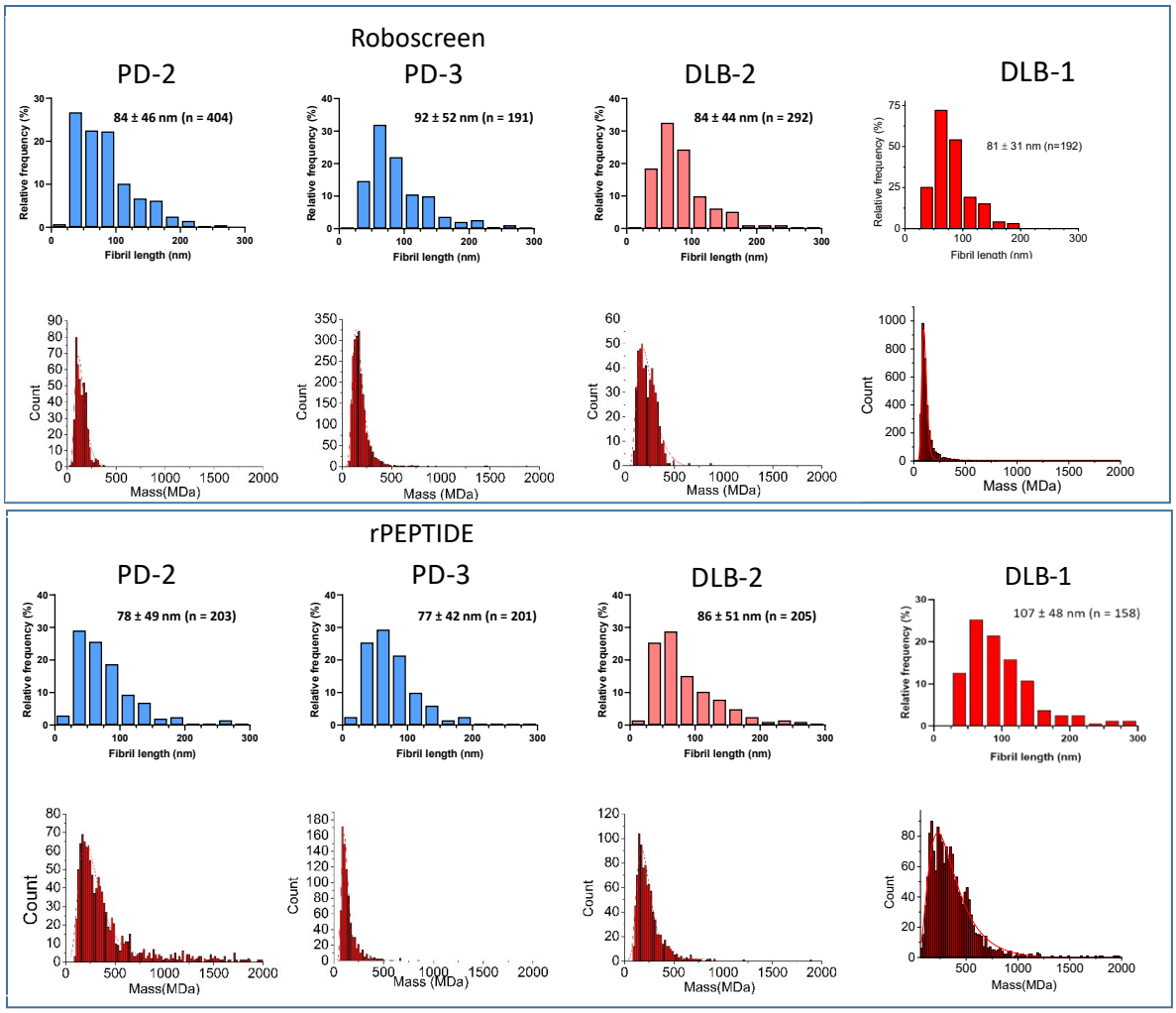


**Figure S3**. Results obtained for two additional PD patients (PD-2 and PD-3) and DLB patients (DLB-1 and DLB-2): mass distributions of amplified fibrils, and corresponding length distributions (extracted from TEM images of amplified fibrils). Details on samples are given in Table S3.

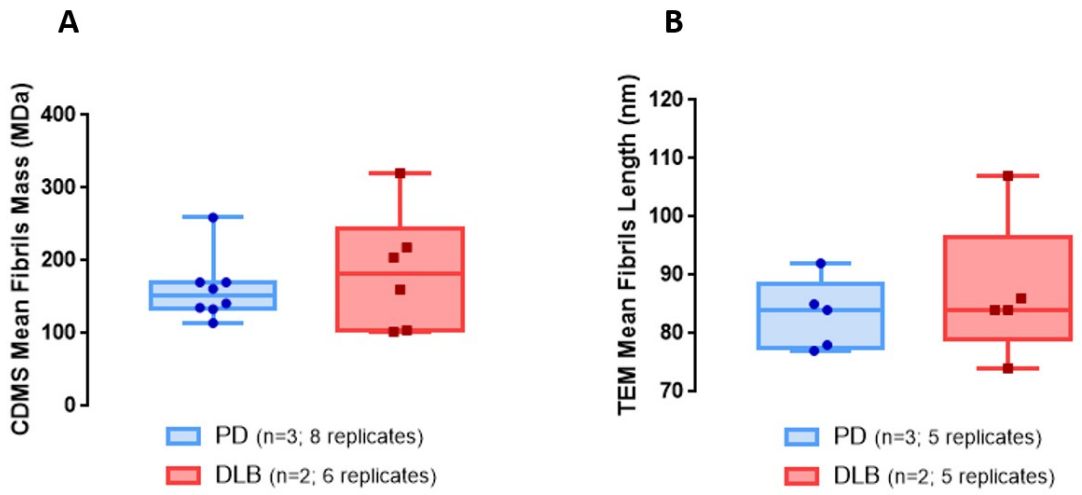


**Figure S4**. Fibrils mean mass (MDa) and mean size (nm) obtained for PD patients (n = 3) and DLB patient (n = 2).

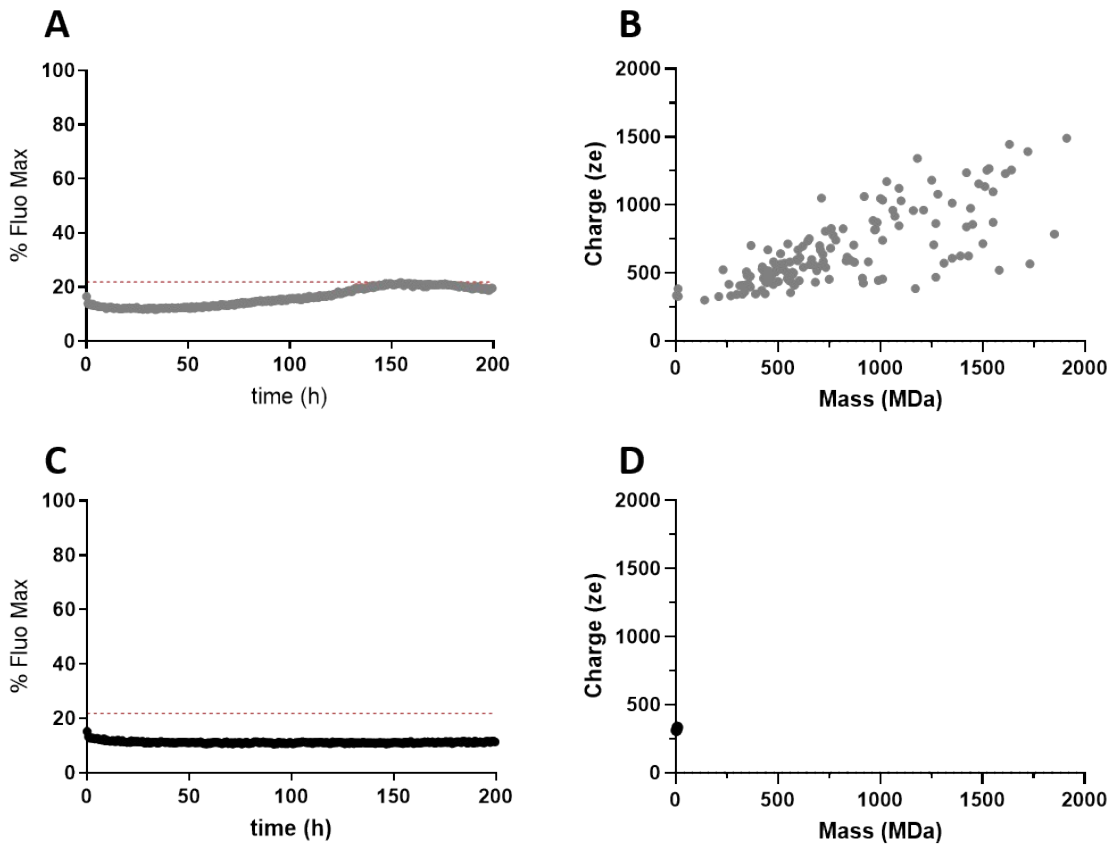


**Figure S5.** ThT detection of αSyn seeding activity in CTL brain homogenate (RT-QuIC, panels A, C) and corresponding charge vs. mass 2D graphs (CDMS, panels B, D). Two individual reaction wells are shown, one suggesting a late and non-specific amplification (A) and the other one showing no amplification (C). Accordingly, CDMS detected few (B) or no (D) fibrils.

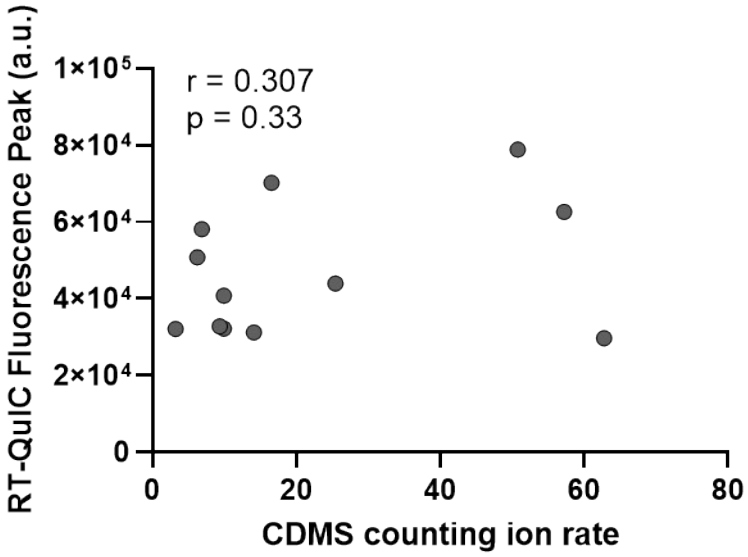


**Figure S6.** Correlation between RT-QuIC fluorescence peak and mass spectrometry counting rate. (Pearson's R=0.307)

| Cohort | | RT-QuIC | | | CDMS | | | TEM | |
|---|---|---|---|---|---|---|---|---|---|
| Etiology | Sample number | Recombinant Protein | ThT Fluorescence Peak (a.u.) | ThT Fluorescence Peak (% Fluo Max) | Mean Mass (Mda) | PDI | Total fibril ions signal rate | Fibrils Length Mean (nm) | Standard deviation (nm) |
| **PD patients (n=3)** | | | | | | | | | |
| PD-1 | A8 | Roboscreen | 109 517 | 100,0 | 170 | 1,26 | | 85 | 45 |
| | B8 | | 62 654 | 57,1 | 135 | 1,08 | 57,23 | | |
| | C8 | | 70 194 | 64,1 | 170 | 1,13 | 16,55 | | |
| | D8 | | 78 899 | 72,0 | 141 | 1,07 | 50,77 | | |
| | E8 | rpeptide | 42 418 | 93,1 | | | | | |
| | F8 | | 31 378 | 68,9 | | | | | |
| | H8 | | 34 144 | 75,0 | | | | | |
| PD-2 | C5 | Roboscreen | 32 236 | 83,4 | 133 | 1,19 | 9,92 | 84 | 46 |
| | F5 | rpeptide | 50 761 | 100,0 | 259 | 1,27 | 6,23 | 78 | 49 |
| PD-3 | C6 | Roboscreen | 31 227 | 80,8 | 161 | 1,13 | 14,11 | 92 | 52 |
| | G6 | rpeptide | 40 791 | 80,4 | 114 | 1,11 | 9,95 | 77 | 42 |
| | | **Mean** | **53 111** | **80** | **160** | **1,15** | **23,54** | **83** | **47** |
| | | **SD** | **24 996** | **14** | **44** | **0,08** | **21,15** | **6** | **4** |
| | | **CV (%)** | **47,1** | **17,7** | **27,7** | **6,9** | **89,9** | **7,3** | **8,2** |
| **DLB patients (n=2)** | | | | | | | | | |
| DLB-1 | A9 | Roboscreen | 99 704 | 91,0 | | | | 74 | 36 |
| | B9 | | 43 917 | 40,1 | 104 | 1,07 | 25,46 | | |
| | C9 | | 29 738 | 27,2 | 102 | 1,06 | 62,76 | 84 | 33 |
| | D9 | | 58 160 | 53,1 | 160 | 1,19 | 6,88 | | |
| | E9 | rpeptide | 33 538 | 73,6 | | | | | |
| | F9 | | 14 543 | 31,9 | 320 | 1,41 | | 107 | 48 |
| | G9 | | 21 037 | 46,2 | | | | | |
| | H9 | | 12 365 | 27,2 | | | | | |
| DLB-2 | B9 | Roboscreen | 32 756 | 84,7 | 218 | 1,23 | 9,37 | 84 | 44 |
| | G9 | rpeptide | 32 089 | 63,2 | 204 | 1,17 | 3,21 | 86 | 51 |
| | | **Mean** | **37 785** | **54** | **185** | **1,19** | **21,53** | **87** | **42** |
| | | **SD** | **25591** | **23** | **82** | **0,13** | **24,56** | **12** | **8** |
| | | **CV (%)** | **67,7** | **43,6** | **44,5** | **10,70** | **114,07** | **13,9** | **18,2** |

**Table S3**. Samples' characteristics for Figures S3-S4 and Figure 2. Summary of measurements results for PD patients (n=3) and DLB patients (n=2). (SD = standard deviation; PD = Parkinson's disease; DLB = disease with Lewy Bodies; PDI = polydispersity index; CV = covariance)

**References**


1. London Neurodegenerative Diseases Brain Bank; MRC UK Brain Banks Network. No. Access: 1, Last: 2015.
2. Montine, T. J.; Phelps, C. H.; Beach, T. G.; Bigio, E. H.; Cairns, N. J.; Dickson, D. W.; Duyckaerts, C.; Frosch, M. P.; Masliah, E.; Mirra, S. S.; Nelson, P. T.; Schneider, J. A.; Thal, D. R.; Trojanowski, J. Q.; Vinters, H. V.; Hyman, B. T., National Institute on Aging–Alzheimer's Association guidelines for the neuropathologic assessment of Alzheimer's disease: a practical approach. *Acta Neuropathologica* **2012,** *123* (1), 1-11.
3. Doussineau, T.; Kerleroux, M.; Dagany, X.; Clavier, C.; Barbaire, M.; Maurelli, J.; Antoine, R.; Dugourd, P., Charging megadalton poly(ethylene oxide)s by electrospray ionization. A charge detection mass spectrometry study *Rapid Communications in Mass Spectrometry* **2011,** *25*, 617.
4. Doussineau, T.; Bao, C. Y.; Clavier, C.; Dagany, X.; Kerleroux, M.; Antoine, R.; Dugourd, P., Infrared Multiphoton Dissociation Tandem Charge Detection-Mass Spectrometry of Single Megadalton Electrosprayed Ions. *Review of Scientific Instruments* **2011,** *82*, 084104.
5. Antoine, R., Weighing synthetic polymers of ultra-high molar mass and polymeric nanomaterials: What can we learn from charge detection mass spectrometry? *Rapid Communications in Mass Spectrometry* **2020,** *34* (S2), e8539.
6. Keifer, D. Z.; Pierson, E. E.; Jarrold, M. F., Charge detection mass spectrometry: weighing heavier things. *Analyst* **2017,** *142* (10), 1654-1671.
7. El-Faramawy, A.; Siu, K. W. M.; Thomson, B. A., Efficiency of Nano-Electrospray Ionization. *Journal of the American Society for Mass Spectrometry* **2005,** *16* (10), 1702-1707.
8. Doussineau, T.; Mathevon, C.; Altamura, L.; Vendrely, C.; Dugourd, P.; Forge, V.; Antoine, R., Mass Determination of Entire Amyloid Fibrils by Using Mass Spectrometry. *Angew. Chem. Int. Ed.* **2016,** *55*, 2340-2344.
9. Alafuzoff, I.; Thal, D. R.; Arzberger, T.; Bogdanovic, N.; Al-Sarraj, S.; Bodi, I.; Boluda, S.; Bugiani, O.; Duyckaerts, C.; Gelpi, E.; Gentleman, S.; Giaccone, G.; Graeber, M.; Hortobagyi, T.; Höftberger, R.; Ince, P.; Ironside, J. W.; Kavantzas, N.; King, A.; Korkolopoulou, P.; Kovács, G. G.; Meyronet, D.; Monoranu, C.; Nilsson, T.; Parchi, P.; Patsouris, E.; Pikkarainen, M.; Revesz, T.; Rozemuller, A.; Seilhean, D.; Schulz-Schaeffer, W.; Streichenberger, N.; Wharton, S. B.; Kretzschmar, H., Assessment of beta-amyloid deposits in human brain: a study of the BrainNet Europe Consortium. *Acta neuropathologica* **2009,** *117* (3), 309-320.